Available online at www.sciencedirect.com
SCIENCE DIRECT
Journal of Solid State Chemistry 179 (2006) 1237–1246
JOURNAL OF SOLID STATE CHEMISTRY
www.elsevier.com/locate/jssc

Defect generation of rutile-type SnO_2 nanocondensates: Imperfect oriented attachment and phase transformation

Wan-Ju Tseng[a], Pouyan Shen[a], Shuei-Yuan Chen[b,*]

[a]*Institute of Materials Science and Engineering, National Sun Yat-sen University Kaohsiung, Taiwan, ROC*
[b]*Department of Mechanical Engineering, I-Shou University Kaohsiung, Taiwan, ROC*

Received 14 November 2005; received in revised form 9 January 2006; accepted 16 January 2006
Available online 21 February 2006

Abstract

The rutile-type SnO_2 nanocondensates as condensed by Nd-YAG laser ablation on Sn target under oxygen background gas were characterized by analytical electron microscopy to have {110}, {100} and {101} facets, which are beneficial for {$\sim hkl$} vicinal attachment to form edge dislocations, faults and twinned bicrystals. The {011}-interface relaxation, by shearing along $\langle 011 \rangle$ directions, accounts for a rather high density of edge dislocations near the twin boundary thus formed. The rutile-type SnO_2 could be alternatively transformed from orthorhombic $CaCl_2$-type structure (denoted as o) following parallel crystallographic relationship, $(0\bar{1}1)_r//(0\bar{1}1)_o$; $[111]_r//[111]_o$, and full of commensurate superstructures and twins parallel to (011) of both phases.

Keywords: SnO_2 condensates; Laser ablation condensation; Defects; Shape; Coalescence; AEM

1. Introduction

Gas evaporation is an effective method of producing ambient dioxide nanoparticles more or less in agglomeration and coalescence. For example, TiO_2 nanoparticles frequently formed chain aggregates due to collisions between small aggregates in Brownian motion [1]. Nanoparticle chain aggregates (NCA) of TiO_2 actually possess elastomeric properties including stretch under tension, and contraction when the tension is relaxed [1]. The coalescence of TiO_2 nanoparticles is also of interest because conventionally brittle ceramics may become ductile permitting large plastic deformation at low temperature if the resultant polycrystal has crystal size in a few nanometers [2]. The ductility may simply originate from the diffusion flow of atoms along the intercrystalline interface.

Recently Nd-YAG-laser pulse irradiation was used to vaporize oxygen-purged Ti target to a more energized state so that α-PbO_2-type TiO_2 [3] and fluorite-type related TiO_2 particles [4] were produced. This novel synthesis route of dense TiO_2 polymorphs sheds light on their possible condensation around stars in addition to terrestrial occurrences as a response to static high pressure in crustal rocks attending subduction into Earth's interior [5] and natural dynamic events in shocked gneisses from the Ries crater in Germany [6].

The interrelated research on the evaporation–condensation synthesis of TiO_2 polymorphs by Nd-YAG laser further showed the coalescence of predominant anatase and rutile nanoparticles to form dislocations, stacking faults and twin [7,8]. The crystal growth and defect generation of titania nanoparticles during condensation is an interesting comparison to imperfect oriented attachment of sol–gel derived anatase crystallites under hydrothermal conditions [9,10].

The present synthesis of SnO_2 by Nd-YAG laser ablation condensation revealed two different mechanisms of defect generation for the rutile-type SnO_2 (cassiterite, space group $P4_2/mnm$). The first mechanism is about imperfect oriented attachment of individual nanoparticles as previously observed for isostructural TiO_2 condensates [7]. The alternative may have something to do with partial transformation from a specific dense structure, i.e. $CaCl_2$-type SnO_2 (space group $Pnnm$), and hence defective as predicted from static compression experiments [11].

*Corresponding author. Fax: +886 7 6578853.
E-mail address: steven@isu.edu.tw (S.-Y. Chen).

0022-4596/$ - see front matter © 2006 Elsevier Inc. All rights reserved.
doi:10.1016/j.jssc.2006.01.035

Rietveld refinements of SnO_2 at high pressure indicated that rutile type underwent second order transformation to form $CaCl_2$-type followed by first order transformation to form α-PbO_2-type (space group *Pbcn*) and then a $Pa\bar{3}$-modified fluorite-type with increasing pressure [11,12]. The defect microstructures observed in the present cassiterite condensates can be rationalized by specific lattice correspondence and distortion associated with the second order transformation from $CaCl_2$ type to rutile type. This is of importance to understand the defect generation mechanism for analogous metal dioxide condensates with rutile-type related structures.

2. Experimental

The tin targets with negligible impurities (99.999% pure) were subject to energetic Nd-YAG-laser (Lotis, 1064 nm in wavelength, beam mode: TEM00) pulse irradiation. The pulse time duration was 240 μs at 10 Hz. Laser beam was focused to a spot size of 0.03 mm^2 on the tin target inside the ablation chamber. Oxygen gas (99.999% purity) at a flow rate of 15–25 L/min was supplied to oxidize and cool the condensates. The *pulse energy* 350, 430, 500, 830, and 1100 mJ/pulse, i.e. *power density of* 4.9×10^7, 6.0×10^7, 7.0×10^7, 1.2×10^8, 1.5×10^8 Watt/cm^2, respectively, *given pulse time duration of 240 μs at 10 Hz and focused area of 0.03 mm^2*, assured a good yield of SnO_2 condensates.

Copper grids overlaid with a carbon-coated collodion film and fixed in position by a holder at a distance of 2.5–10 mm from the target were used to collect the condensates. The composition and crystal structures of the SnO_2 condensates were characterized by analytical electron microscopy (AEM, JEOL 3010 instrument at 300 keV) with selected area electron diffraction (SAED), and point-count energy dispersive X-ray (EDX) analysis at a beam size of 10 or 15 nm. Bright field images (BFI) taken by transmission electron microscopy (TEM) were used to study the general morphology and agglomeration of the condensed SnO_2 particles. Lattice imaging coupled with two-dimensional (2-D) Fourier transform and inverse transform were used to analyze the defects and crystal structure of nano-size particles. The *d*-spacings measured from SAED patterns were used for least-squares refinement of the lattice parameters.

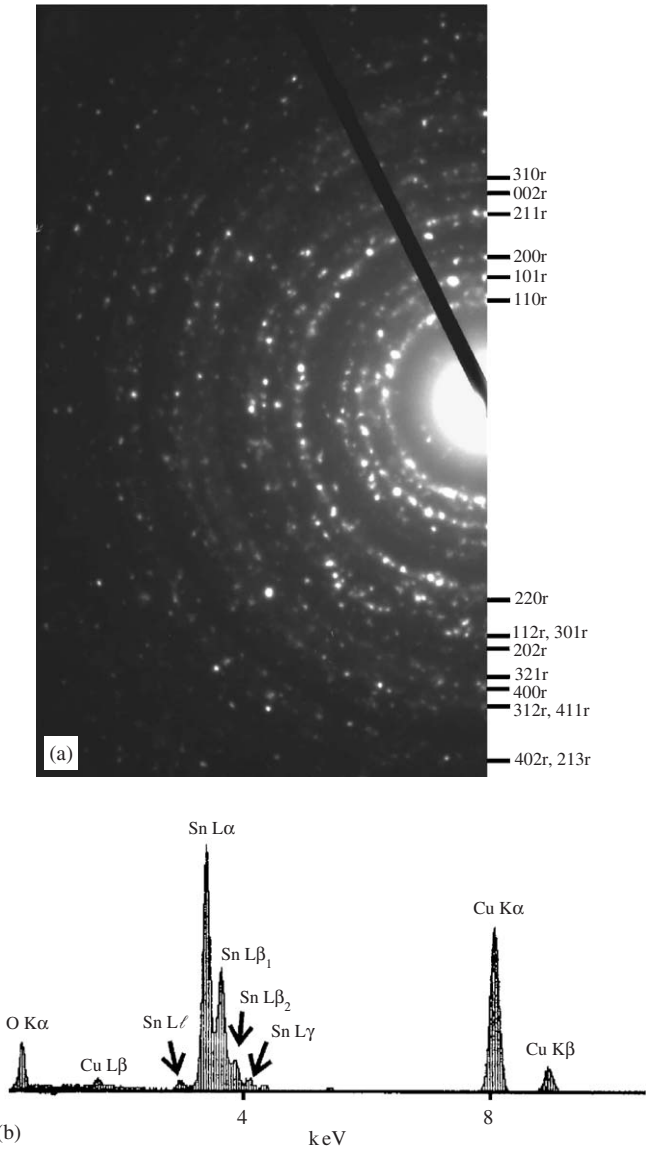

Fig. 1. (a) SAED pattern of randomly oriented SnO_2 condensates taken at 300 kV with a selected area aperture of 1 μm. The condensates are predominantly rutile-type structure as indicated by the strong ring diffractions (*hkl*) indexed. Minor dense polymorphs will be reported elsewhere. (b) EDX analysis of a representative SnO_2 particle showing strong Sn and O peaks, with Cu peaks from supporting Cu ring. Sample produced by laser ablation at 0.5 J/pulse and oxygen flow rate of 15 L/min.

3. Results

3.1. Structure and composition of the condensates

Laser ablation condensation at 0.35–1.1 J/pulse and oxygen flow rate of 15–25 L/min produced nanometer-size and randomly oriented SnO_2 particles which are predominantly rutile-type, as indicated by SAED pattern of the representative sample produced at 0.5 J/pulse and oxygen flow rate of 15 L/min (Fig. 1a). Minor dense phase not relevant to this article will be reported elsewhere. The rutile-type structure of the SnO_2 condensates was also identified by 2-D Fourier transform of the individual particles as shown later. X-ray diffraction (XRD) trace of the condensates accumulated on silica glass substrate at 500 mJ/pulse and oxygen flow rate of 30 L/min for 10 min (Appendix) indicated the rutile-type structure was indeed predominant for SnO_2. Additional Sn and SnO phases occurred in the accumulated deposit with oxygen deficiency, but not in the TEM samples with sufficient oxygen uptake during condensation. The (110), (101), (200), (211) diffractions of rutile-type condensates have strong to moderate strong intensity and *d*-spacings of 0.3366, 0.2650, 0.2377, 0.1768 nm, respectively, as measured from

the XRD trace. These *d*-spacings are consistent with the ambient lattice parameters ($a = 0.4738$ nm and $c = 0.3187$ nm, JCPDS file 21-125) for the rutile-type SnO_2 indicating negligible residual stress and impurities for the present condensates.

EDX analysis of the SnO_2 condensates in TEM samples always showed strong Sn and O peaks with fixed count ratio (Fig. 1b) regardless of oxygen flow rate employed in the condensation process. In fact, the rutile-type SnO_2 condensates have stoichiometric composition based on the counts ratio of Sn and O using commercial cassiterite powders (99.9%, Acros Company) as standard.

3.2. Shape and defects of the condensates

BFI taken at 50,000 × and 120,000 × (Fig. 2a and b) for the representative sample fabricated at 0.5 J/pulse and oxygen flow rate of 15 L/min showed the SnO_2 nanoparticles formed both NCA and compact aggregates. The shape and defects of the individual SnO_2 nanoparticles with rutile structure were revealed by lattice image. The rutile-type nanoparticle has well-developed {110} facets as shown by the representative lattice image in Fig. 3a. 2-D Fourier transform in [001] zone axis (Fig. 3b) and the reconstructed image (Fig. 3c) from the square region in Fig. 3a showed dislocations with half plane parallel to {110}. Fig. 4 showed another rutile-type nanoparticle about 30 nm in size with well-developed {100} in addition to {110} faces. The reconstructed image of this particle also showed edge dislocation with half plane parallel to {110} (Fig. 4b). The {110} half plane was also reported for the analogue TiO_2 rutile in the synthetic condensates [7] and natural occurrence [13]. The rutile-type nanoparticles with {110} faces tended to coalesce over a specific $(10\bar{1})$ surface to form twinned bicrystals with different diffraction contrast across the twin boundary (Fig. 5a). 2-D Fourier transform from the square region in Fig. 5a showed twinned diffraction spots in [111] zone axis (Fig. 5b). The inverse transform gives the reconstructed image (Fig. 5c) from the square region in Fig. 5a showing a rather high density of dislocations near the twin boundary.

Some of the rutile-type nanoparticles showed rather complicated defects. For example, 2-D Fourier transform and reconstructed image (Figs. 6b and c, respectively) from region I in Fig. 6a, showed intimate mixture of rutile-type structure with 3 × commensurate superstructures and polysynthetic twinning parallel to the (011) plane, as well as a possible relic of orthorhombic $CaCl_2$-type structure (denoted as o) following parallel crystallographic relationship, $(0\bar{1}1)_r//(0\bar{1}1)_o$; $[111]_r//[111]_o$. 2-D Fourier transform (Fig. 6d) and reconstructed image (Fig. 6e) from region II showed fine twin domains and dislocations, which can be attributed to coalescence, deformation and/or transformation as discussed later.

The lattice fringes of rutile-type nanoparticle showed faults and dislocations near the amorphous region (Fig. 7). The amorphization of rutile-type structure may be attributed to electron irradiation and/or relaxation of the lattice with residual stress upon cooling of the condensates. Alternatively, transformation from $CaCl_2$ type to rutile type may possibly cause dislocation avalanche and hence amorphization.

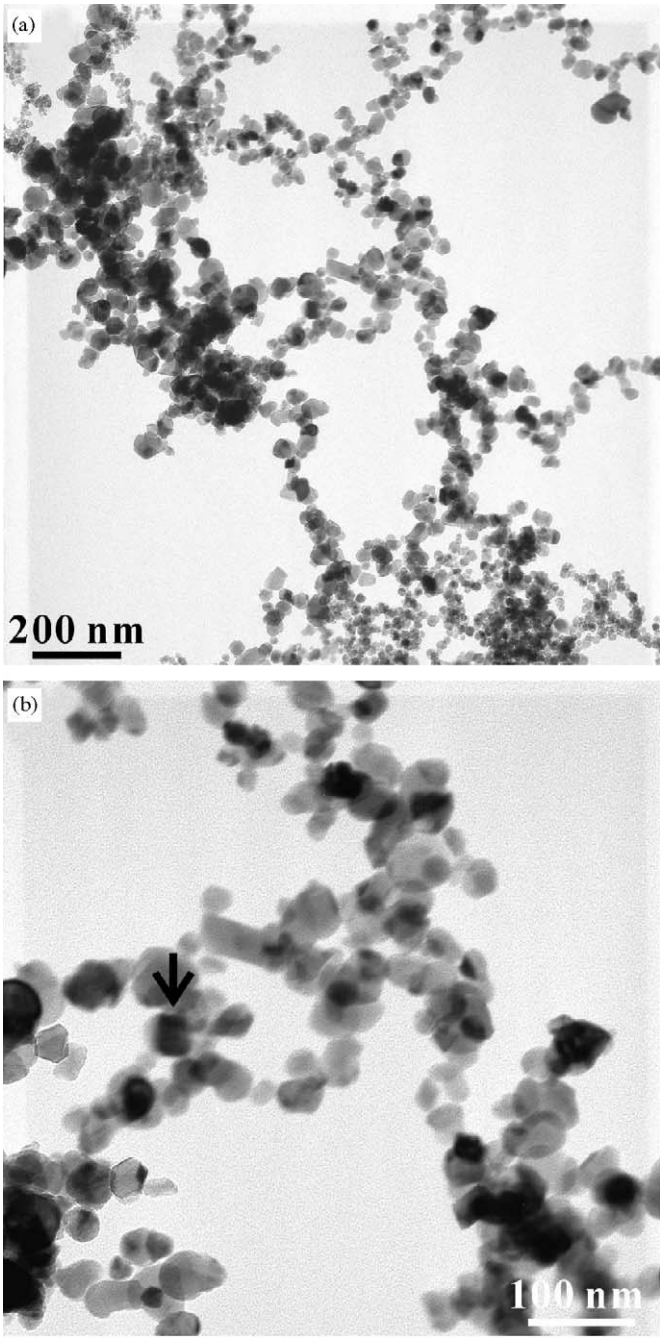

Fig. 2. TEM BFI (a) and (b) taken at 50,000 × and 120,000 ×, respectively, showing equant particles assembled as NCA and cubic particle denoted by an arrow. The same specimen as Fig. 1.

3.3. Size distribution of the condensates

Particle size was estimated on BFI at 25,000 × in area with more than 110 particles. Note the aspect ratio of the

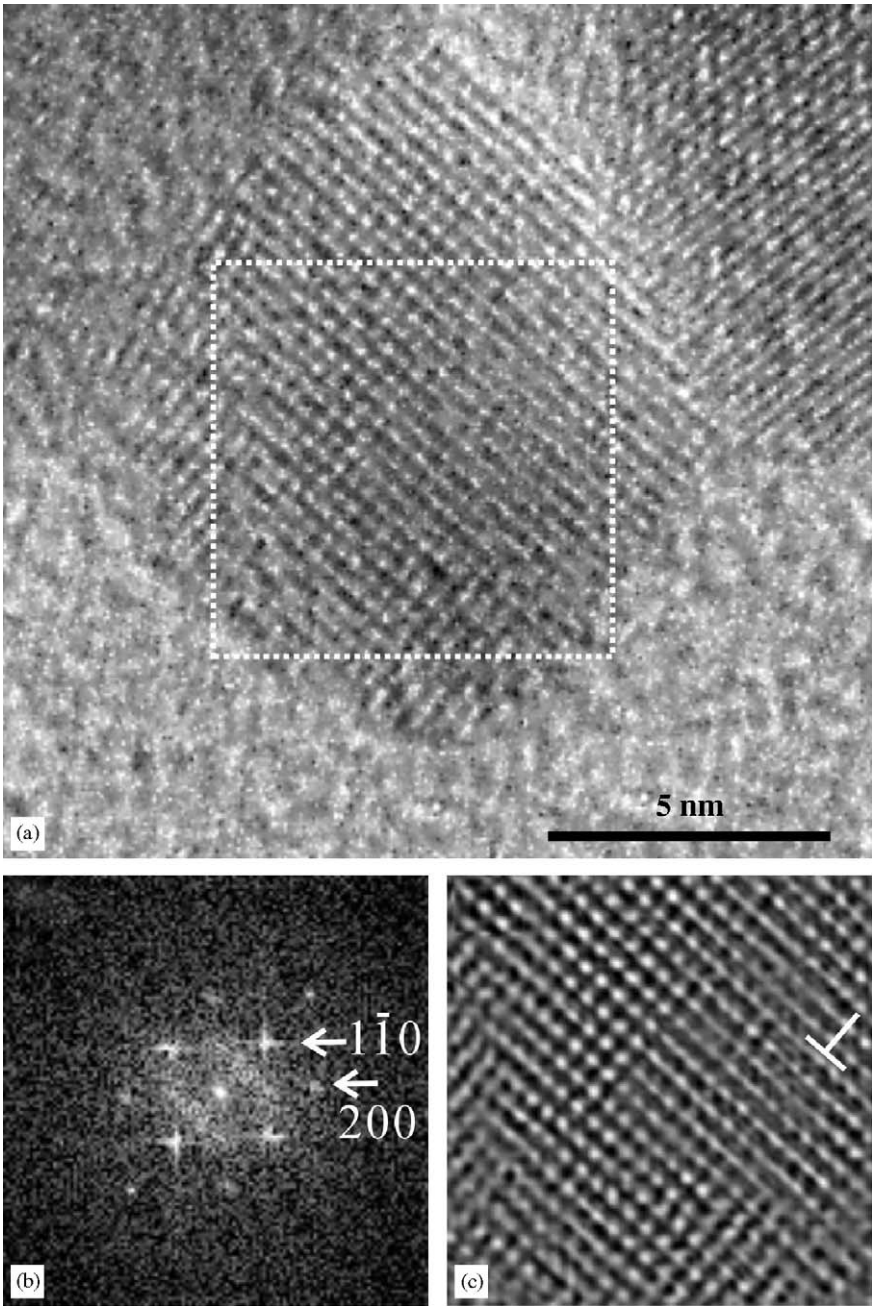

Fig. 3. (a) Lattice image of a rutile-type SnO_2 nanoparticle about 10 nm in size with well-developed {110} faces. (b) 2-D Fourier transform in [001] zone axis and (c) reconstructed image from the square region in (a) showing dislocations (denoted by T) with half plane parallel to (110). Sample produced by laser ablation at 1.1 J/pulse and oxygen flow rate of 20 L/min.

particles ranges from 1.2 to 1.8, and the maximum length of the particles was taken as the particle size. The size distribution for the representative case of 0.5 J/pulse and 15 L/min flow rate of O_2 was constructed as a histogram with fitted curve (Fig. 8). In fact, the average particle size is independent of laser power input but increases slightly with the increase of oxygen flow rate. A more sufficient background gas would in fact shorten the mean free path of the energized atoms and plasma in order to nucleate the crystalline clusters and would increase oxygen surface diffusion for the clusters to grow [14].

4. Discussion

4.1. Effect of radiant heating on condensates coagulation

Radiant heating still prevailed after the crystallites were condensed in a Derjarguin laser process. This was manifested by thermally activated coagulation and coalescence of nanoparticle in the aggregates. Aerosol agglomerates are often formed by collision between primary particles, which can range from a few to several tens of nanometers [15]. The structure of the agglomerates can be

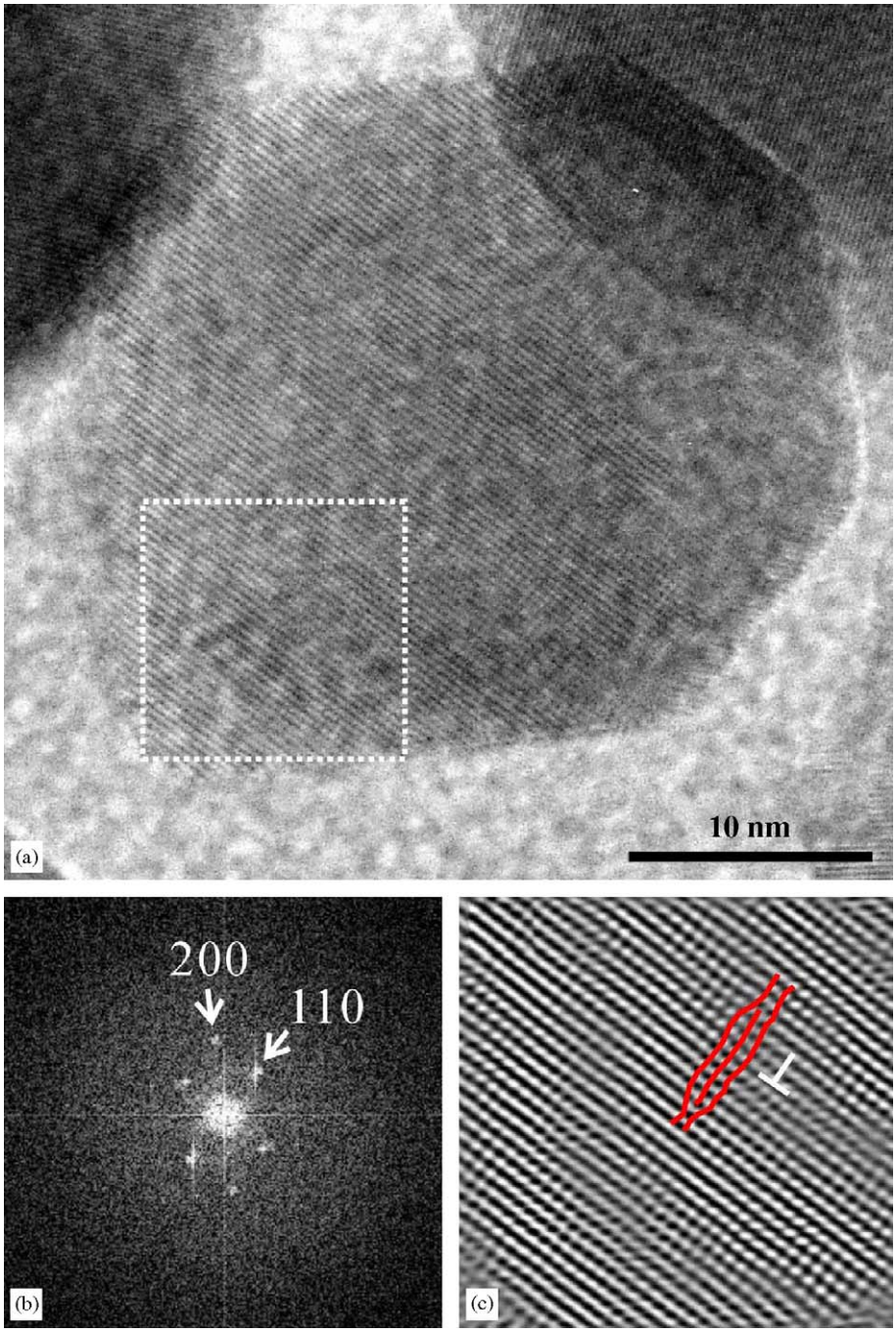

Fig. 4. (a) Lattice image of a rutile-type SnO_2 nanoparticle about 30 nm in size with well-developed {110} and {100} faces in [001] zone axis. (b) 2-D Fourier transform and (c) reconstructed image from the square region in (a) showing dislocation (denoted by T) and fault (denoted by red lines) with extra plane parallel to $(1\bar{1}0)$. Sample produced by laser ablation at 1.1 J/pulse and oxygen flow rate of 20 L/min.

described by a power law relation between the number of primary particles per agglomerate and a characteristic agglomerate diameter. The exponent in this power law signifies a specific agglomerate structure and is called the fractal dimension [16]. A model was introduced to describe the kinetics of the restructuring of aerosol aggregates during in situ heating in the gas phase [16], assuming that the restructuring coefficient is of an Arrhenius form

$$(d_p/d_o)D_f = k(d_{cl}/d_o), \quad (1)$$

where d_o is the primary particle diameter, d_p the mobility diameter of the aggregate before the heating process, D_f fractal dimension, k is a proportionality constant, and d_{cl} the mobility diameter of the close-packed aggregate.

The titania condensates produced by gas evaporation method as the form of NCA possess elastomeric properties [1]. Briefly speaking, chain stretching occurs by breaking weak van der Waals bonds between the particles in the NCA kinks, leading to formation of a nearly straight chain in a state of higher potential energy. On the other hand,

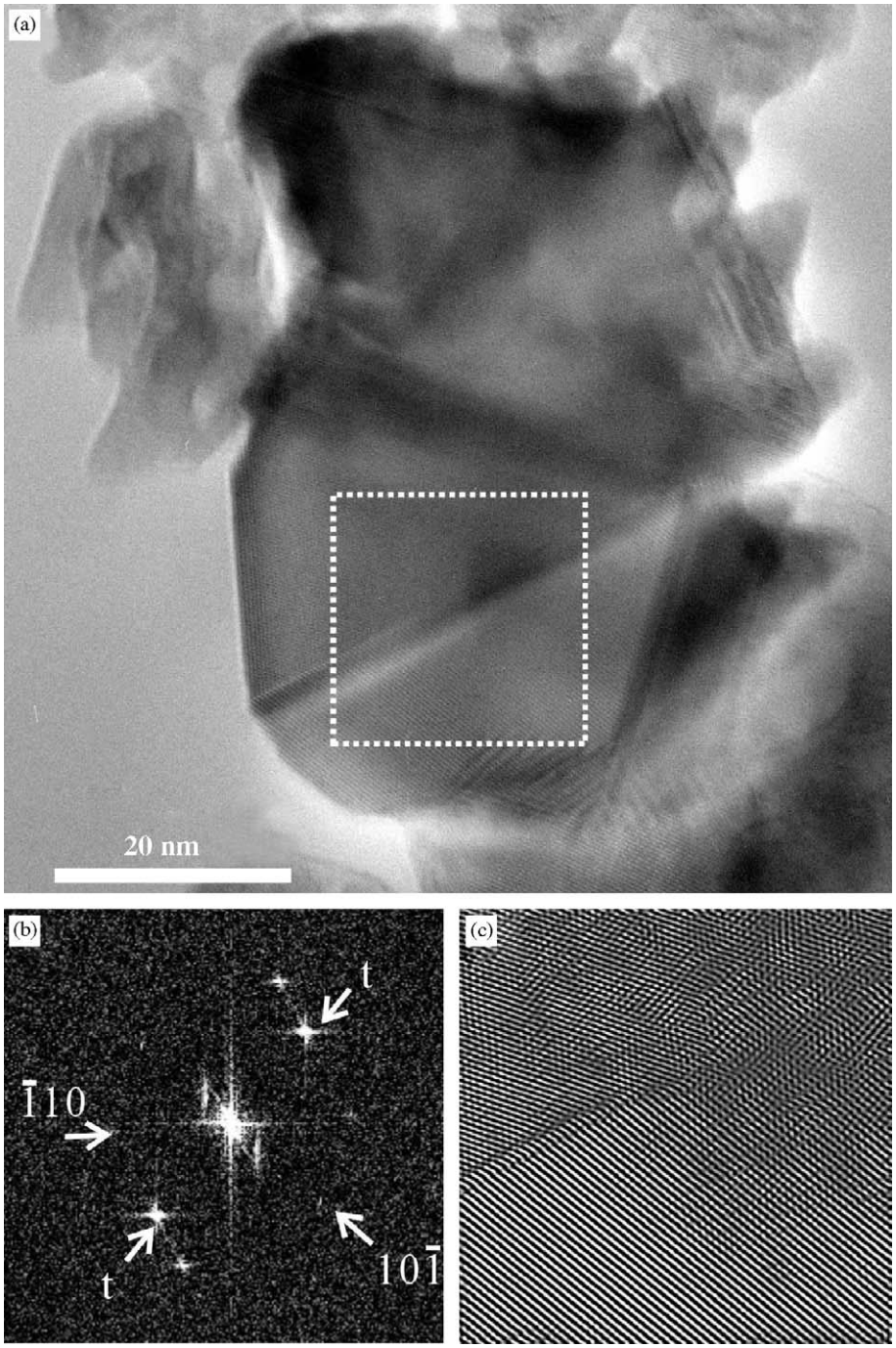

Fig. 5. (a) Lattice image of rutile-type SnO_2 nanoparticles with {110} and {101} faces in [111] zone axis, which were coalesced over a specific $(10\bar{1})$ contact plane to form twinned bicrystals. (b) Fourier transform, with the (*hkl*) of a variant labeled and the twinned spots denoted by t, and (c) reconstructed image from the square region in (a) showing a rather high density of dislocations near the twin boundary. Sample produced by laser ablation at 0.83 J/pulse and oxygen flow rate of 20 L/min.

van der Waals force makes the NCA kinks when tension is relaxed. When titania nanoparticles coagulated as NCA or other fractal dimensions are heated, considerable reconstruction toward close packing could occur. For example, D_f was estimated to be 2.33–3.00 from 20 to 1000 °C for titania aggregates in a gas evaporation process [17]. Regardless of oxygen flow rate in the laser ablation process, titania condensates always formed aggregates in NCA and close packed manner with D_f approaching 3 [18]. Thus, considerable reconstruction of titania nanoparticle aggregates, at temperatures as high as near 1000 °C under the influence of gray body radiation, has occurred during such a laser ablation process. Since the same laser ablation process was adopted in the present condensation of the

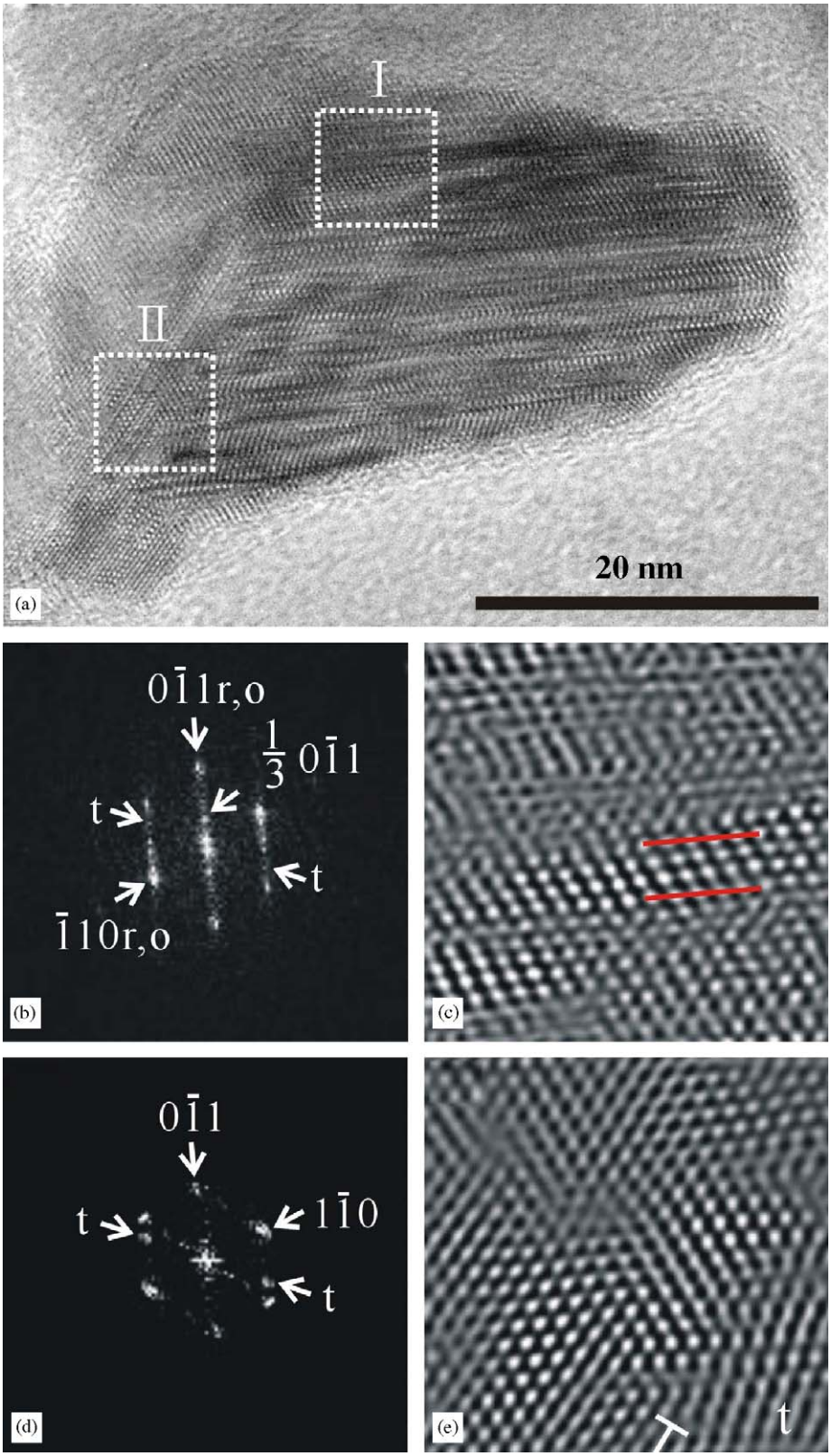

Fig. 6. (a) Lattice image of two SnO_2 nanoparticles coalesced to form twinned bicrystals in [111] zone axis of the rutile-type structure. (b,d) 2-D Fourier transform and (c,e) reconstructed images from the highly defective particle (region I) and the bicrystal twin boundary (region I), respectively. As represented by region I, the rutile-type SnO_2 particle (denoted as r) was intimately mixed with $3\times$ commensurate superstructure (delineated by red lines) and a possible relic of orthorhombic $CaCl_2$-type structure (denoted as o) following parallel crystallographic relationship (cf. text). The twin domains are denoted by t and dislocation by T. Sample produced by laser ablation at 1.1 J/pulse and oxygen flow rate of 20 L/min.

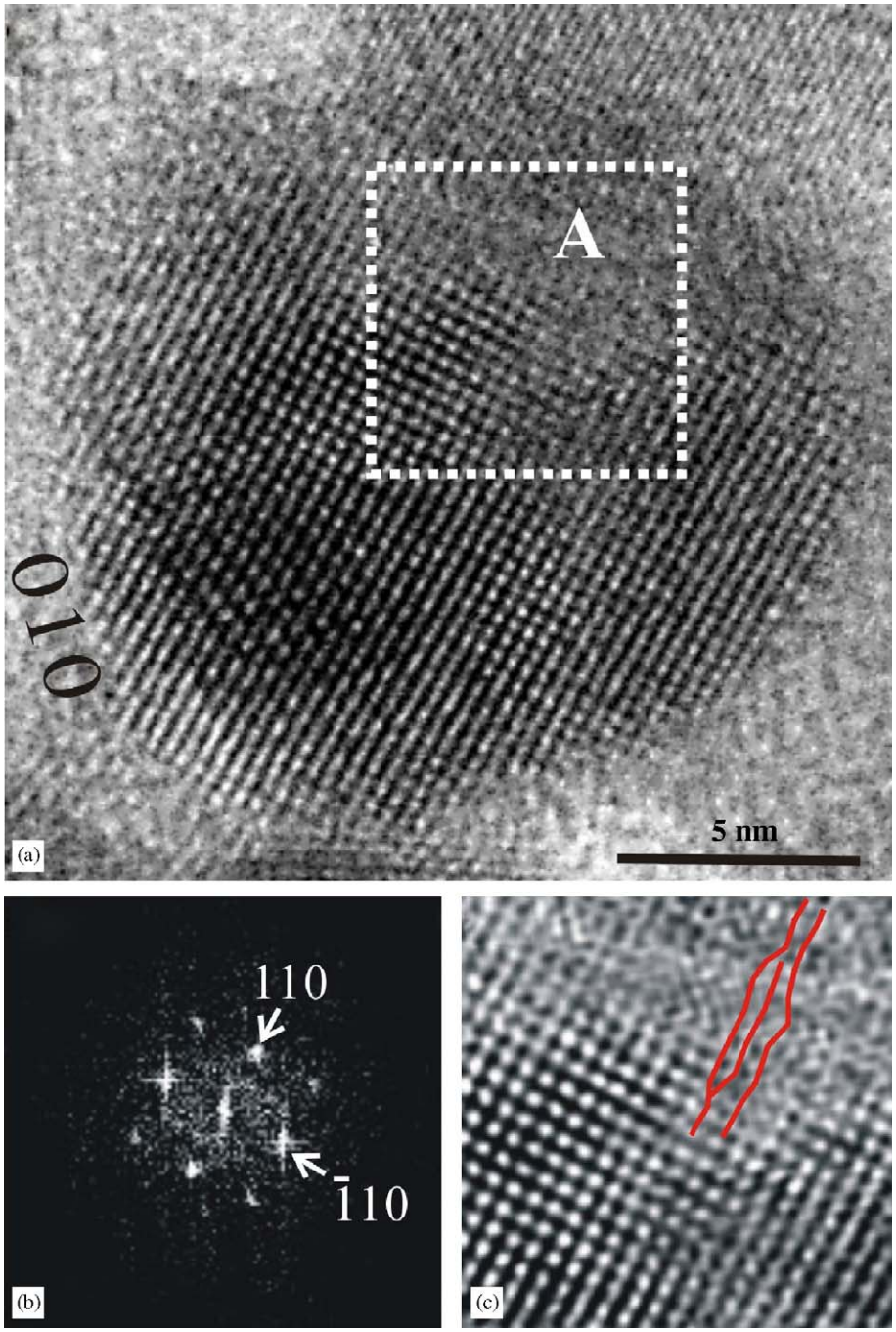

Fig. 7. (a) Lattice image of a rutile-type SnO_2 nanoparticle about 15 nm in size with {01} and {110} facets and partially amorphized region denoted by A. (b) 2-D Fourier transform in [001] zone axis and (c) reconstructed image from the square region in (a) showing faults/dislocations denoted by red lines in partially amorphized region. Sample produced by laser ablation at 1.1 J/pulse and oxygen flow rate of 20 L/min.

SnO_2, the NCA is expected to experience the same level of radiant heating to form a close packed manner.

4.2. Coalescence twin

Rapid cooling of the condensates under the influence of oxygen background gas may possibly cause crystal deformation and hence lattice imperfections. However, the fact that the dislocations are enriched near specific contact planes parallel to the well-developed surface, implies an alternative mechanism of defect generation. Coalescence of crystallites over a specific contact plane was known to cause twins, such as (111)-specific coalescence twinning for fluorite-type CeO_2 condensates [19] and t-ZrO_2 [20], and (011)-specific coalescence twinning for rutile TiO_2 [7].

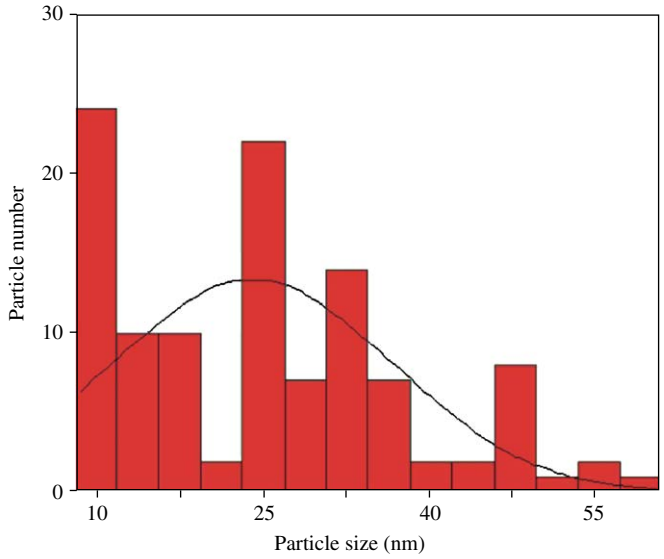

Fig. 8. Histogram with curve fitting showing the size distribution of SnO_2 condensates produced by laser ablation at 0.5 J/pulse and oxygen flow rate of 15 L/min based on five independent BFIs taken at 25,000 × .

The planar defects of the present rutile-type SnO_2 condensates can also be accounted for by imperfect attachment of the nanoparticles over specific surfaces. The rutile-type SnO_2 nanoparticles do have well-developed {011} surfaces beneficial to {011} vicinal attachment in order to be unified or to form twin plane, depending on the orientation of the adjoined particles. Such a coalescence twin indicates an energy cusp for the {011} twin plane of the rutile-type SnO_2.

The present SnO_2 nanocondensates also showed rather efficient coalescence via arbitrary impinged corner, rather than specific low-index contact plane. The attached nanoparticles may form noncoherent interface and then bifurcated toward parallel epitaxy vs. twinning relationship via Brownian rotation of the joined particles. These observations support theoretical consideration of so-called grain rotation coalescence [21]. In such model, the two neighboring grains would finally assume the same orientation [21] because of anisotropic grain boundary energy [22,23]. Twin plane relaxation via crystallographic shear accounts for a high density of dislocations, faults and even commensurate superstructure near the twin boundary. Further study is required to clarify whether unification via corner attachment involved also interface relaxation upon grain rotation coalescence.

4.3. Deformation and transformation induced defects

Brittle ceramics may become ductile permitting large plastic deformation at low temperature if the resultant polycrystal has crystal size in a few nanometers [2]. The ductility may simply originate from the diffusion flow of atoms along the intercrystalline interface of the adjoined SnO_2 nanocondensates.

The plastic deformation of the rutile-type SnO_2 could be alternatively induced by phase transformation as experimentally proved for ceramic single crystals [24]. Transformation from $CaCl_2$-type to rutile type, i.e. space group change from *Pnnm* to $P4_2/mnm$, involves glide plane loss yet 4-fold screw axis gain, given the parallel crystallographic relationship as mentioned. The parallel crystallographic relationship for the two phases is due to closely related crystal structure via a slight polyhedral distortion, in fact a second order type transformation of the polymorphs [11].

The relaxation of the $CaCl_2$/rutile-type interface and/or deformation of the two lattices via crystallographic shear may cause polysynthetic twins, rather than twinned bicrystals, in order to more effectively relieve the residual stress. Such a deformation twinning process was accompanied by the formation of a high density of dislocations, faults and even commensurate superstructure for the composite nanoparticles as mentioned. It is not clear if such transformation/deformation twinning for SnO_2 polymorphs would cause so called transformation toughening as for analogue ZrO_2 materials under the influence of matrix constraint or chemical doping effect [25].

5. Conclusions

The rutile-type SnO_2 nanocondensates as condensed by Nd-YAG laser ablation on Sn target under oxygen background gas have {110}, {100} and {101} facets for {∼*hkl*} vicinal attachment to form edge dislocations, faults and twin bicrystals. Alternatively the rutile-type SnO_2 was likely transformed from orthorhombic $CaCl_2$-type structure following specific crystallographic relationship and hence full of commensurate superstructures, twins, faults, dislocations, and amorphous region.

Acknowledgments

We thank M.H. Tsai for technical assistance on laser ablation and L.J. Wang for technical assistance on AEM and an anonymous referee for constructive comments. Supported by Center for Nanoscience and Nanotechnology at NSYSU and National Science Council, Taiwan, ROC under contracts NSC94-2120-M110-001 and NSC94-2216-E-214-008.

Appendix A. Supplementary data

Supplementary data associated with this article can be found in the online version at doi:10.1016/j.jssc.2006.01.035.

References

[1] S.K. Friedlander, H.D. Jang, K.H. Ryu, Appl. Phys. Lett. 72 (1998) 173.

[2] J. Karch, R. Birringer, H. Gleiter, Nature 330 (1987) 556.
[3] S.Y. Chen, P. Shen, Phys. Rev. Lett. 89 (2002) 096106-1.
[4] S.Y. Chen, P. Shen, Jpn. J. Appl. Phys. 43 (2004) 1519.
[5] S.L. Hwang, P. Shen, H.T. Chu, T.F. Yui, Science 288 (2000) 321.
[6] A. El Goresy, M. Chen, L. Dubrovinsky, P. Gillet, G. Graup, Science 293 (2001) 1467.
[7] M.H. Tsai, S.Y. Chen, P. Shen, Nano Lett. 4 (2004) 1197.
[8] M.H. Tsai, S.Y. Chen, P. Shen, J. Aerosol Sci. 36 (2005) 13.
[9] R.L. Penn, J.F. Banfield, Science 281 (1998) 969.
[10] R.L. Penn, J.F. Banfield, Geochimica et Cosmochimica Acta 63 (1999) 1549.
[11] J. Haines, J.M. Léger, Phys. Rev. B 55 (1997) 11144.
[12] J. Haines, J.M. Léger, O. Schulte, Science 271 (1996) 629.
[13] P. Shen, S.L. Hwang, H.T. Chu, T.F. Yui, C. Pan, W.L. Huang, Eur. J. Mineral 17 (2005) 543–552.
[14] D. Walton, J. Chem. Phys. 37 (1962) 2182.
[15] W. Koch, S.K. Friedlander, J. Colloid Interf. Sci. 140 (1990) 419.
[16] A.P. Weber, S.K. Friedlander, J. Aerosol Sci. 28 (1997) 179.
[17] H.D. Jang, S.K. Friedlander, Aerosol Sci. Technol. 29 (1998) 81.
[18] M.H. Tsai, M.S. Thesis, National Sun Yat-sen University, Taiwan, ROC, 2002.
[19] W.H. Lee, P. Shen, J. Cryst. Growth 205 (1999) 169.
[20] P. Shen, W.H. Lee, Nano Lett. 1 (2001) 707.
[21] D. Moldovan, V. Yamakov, D. Wolf, S.R. Phillpot, Phys. Rev. B 89 (2002) 206101-1-204101-4.
[22] F.J. Humphreys, M. Hatherly, Recrystallization and Related Annealing Phenomena, Pergamon, Oxford, 1995.
[23] K.E. Harris, V.V. Singh, A.H. King, Acta Mater. 46 (1998) 2623.
[24] J.P. Poirier, Creep of Crystals, Cambridge University Press, Cambridge, 1985, p. 260.
[25] D.J. Green, R.H.J. Hannik, M.V. Swain, Transformation Toughening of Ceramics, CRC Press, Boca Raton, FL, 1989, pp. 1–232.